https://doi.org/10.1016/j.apsusc.2018.09.027

Improving the wear and corrosion resistance of CoCrMo-UHMWPE articulating surfaces in the presence of an electrolyte

W. Zai [a,b], M.H. Wong [a], H.C. Man [a,*]

[a] Department of Industrial and Systems Engineering, The Hong Kong Polytechnic University, Hong Kong, China

[b] College of Materials Science and Engineering, Jilin University, Jilin, China.

*E-mail: hc.man@polyu.edu.hk

Abstract

Metal-polymer articulating pairs are common in engineering applications. The present study aims at improving the wear resistance of the polymeric part and the wear-corrosion resistance of the metallic part in the CoCrMo-UHMWPE (ultrahigh-molecular-weight polyethylene) pair. To achieve this end, magnesia-stabilized zirconia coating was fabricated on CoCrMo alloy via a sol-gel route while multi-layer graphene flakes (G) were incorporated in the UHMWPE matrix. Results of the linear reciprocating wear test between the articulating members in bovine serum at 37 °C for 10^6 cycles show significant improvement in tribological behavior of UHMWPE and in corrosion resistance of CoCrMo under abrasive wear. The coefficient of friction and wear mass loss were both reduced to about one half as compared with those between the untreated members. The improvement in wear resistance could be attributed to the presence of graphene in the UHMWPE matrix, which acted as a reservoir of solid lubricant. Electrochemical impedance spectroscopy (EIS) measurements before and during the wear test showed significantly higher corrosion resistance of CoCrMo-ZrO_2 as compared with bare CoCrMo, attributable to the hard and inert ZrO_2 coating. The present work demonstrates a rational materials design for improving the wear and corrosion performance of the CoCrMo-UHMWPE articulating pair.

Keywords: CoCrMo; Sol-gel ZrO_2; UHMWPE; Graphene; Sliding wear; Corrosion

1. Introduction

The use of a metallic part and a polymeric part in an articulating pair is common in engineering applications [1]. As an example in biomedical engineering, an artificial hip joint employs a metal-polymer articulating pair, with CoCrMo alloy as the metallic part and UHMWPE (ultrahigh-molecular-weight polyethylene) as the polymeric part [2-4]. In applications where there is relative sliding motion between the articulating surfaces, wear of the polymeric part and corrosion of the metallic part (if an electrolyte is present) are major causes of malfunctioning and would drastically shorten the service life of the pair [5,6].

While there are different methods of combating failure arising from wear and corrosion damage in a metal-polymer articulating pair, surface modification has been a favorable one as it does not affect bulk mechanical properties [7]. Diamond-like carbon coating on CoCrMo was reported by a number of researchers [8-10] and sol-gel bioactive glass coating was investigated by Mu et al. [11] while ion implantation [12-14] and ultrasonic impact treatment [15] on CrCoMo were attempted by some others. Though such coatings were able to improve the wear resistance of CoCrMo head in abrasion against UHMWPE, the wear damage of UHMWPE was not reduced, as reported in [16]. On the other hand, Roy et al. [17] reported better performance of zirconia femoral head than CoCr femoral heads in bringing a lower wear rate of the UHMWPE counterpart. Li et al. [18] reported zirconia-graphene composite coating prepared by plasma spraying, which showed reduced wear rate in dry sliding wear test against alumina. These previous works suggest that zirconia coating is a potential ceramic coating material for CoCrMo in articulating with another surface. In particular, zirconia has a modulus close to that of metallic alloys, which would thus lower the stress at the coating-substrate interface when used as coating and hence result in better adhesion. On the other hand, modification of UHMWPE for use in the CoCrMo-UHMWPE pair is less commonly reported [19,20].

The present study aims at improving the wear resistance between these two components via a rational materials design. To achieve this end, magnesia-stabilized zirconia coating was fabricated on CoCrMo via a sol-gel route while multi-layer graphene flakes (G) were incorporated in the UHMWPE matrix. The incorporated graphene would serve as a solid lubricant [21] and the zirconia coating on CoCrMo is expected to reduce the friction and wear between the articulating surfaces. The zirconia coating would also protect the metal substrate in abrasive wear in an

electrolyte, such as body fluid, and hence minimize metal ion release by wear induced corrosion. The present study only refers to artificial hip joint and CoCrMo-UHMWPE as an example of metal-polymer articulating pair. As such, biocompatibility study is not the focus and has not been investigated.

2. Experimental methods

2.1 Preparation of UHMWPE-G composite

UHMWPE powder (GUR 1020) with an average molecular mass of 3.5×10^6 g/mol and density of 0.93 g/cm^3 was supplied by Ticona (America). Multi-layer graphene flakes (G) synthesized by mechanical exfoliation with an average diameter of 5-50 μm and thickness of 4-8 nm were supplied by HENQU (China). Graphene flakes were added to alcohol and the suspension was ultrasonicated for 30 min, followed by vigorous stirring for another 30 min to achieve uniform dispersion of graphene flakes in suspension. Different amounts of UHMWPE powder were then added to the suspension and stirred for 30 min to obtain a uniform mixture with different graphene contents (in wt%: 0, 0.1, 0.2, 0.5, 1 and 2%). The UHMWPE-G mixture was then put into an oven at 60 °C for 12 h to remove residual alcohol from the mixture. The dried UHMWPE-G mixtures were hot-pressed at 5 MPa at 100 °C for 1 h and then 20 MPa at 200 °C for 1 h to obtain UHMWPE-G composites.

2.2 Sol-gel coating of MgO-stabilized ZrO2 on CoCrMo substrate

The starting precursor zirconium (IV) n-propoxide ($Zr(OPr)_4$) (70% wt% in 1-propanol, Aldrich), and magnesium acetate tetra-hydrate (MgAc, Aldrich) were dissolved in n-propanol (PrOH). A certain amount of water was added to the solution for $Zr(OPr)_4$ for hydrolyzation. A chelating agent, acetylacetone (AcAc), was used to reduce the reactivity of $Zr(OPr)_4$ alkoxide with water and to control the rate of formation of hydroxide. In this work, the molar ratio of $Zr(OPr)_4$:H_2O:PrOH:AcAC:MgAc was set as 1:5:20:0.8:0.11 [22]. The solution was stirred for 30 min to ensure homogeneous mixing. As early addition of water into the solution might cause hydrolysis of $Zr(OPr)_4$ and precipitation, water was added to the solution dropwise under vigorous stirring as the final step in preparing the precursor solution. After stirring for 3 h at room temperature, a clear precursor solution was obtained.

CoCrMo plates (composition in wt%: 64.2% Co, 28.8% Cr, 6.0% Mo, with minute amounts of Si, Mn, C and trace amounts of Ni and Fe, conforming to ASTM F75) of 10

mm × 50 mm were cut from a sheet of 1 mm thick (supplied by ShiLian Industrial Co., Shanghai, China) and mechanically polished using silicon carbide sandpapers from 360 to 2000 grit to obtain mirror finish. The plates were washed in distilled water, ultrasonically degreased with acetone and then dried at room temperature for 30 min. For sol-gel coating, the plates were dipped in the precursor solution and withdrawn at a speed of 10 cm/min. The coated samples were dried under ambient condition for 30 min and then dried in an oven at 80 °C overnight. The coated samples were then sintered at different temperatures (from 300 °C to 700 °C) for 2 h with a heating rate of 10 °C/min. Samples with different sintering temperatures (300 °C, 500 °C, and 700 °C) were designated as T300, T500, and T700, respectively.

2.3 Microstructural Characterization

To study the phases present in the ZrO_2 coatings on CoCrMo, X-ray diffraction (XRD) experiment was performed using an X-ray diffractometer (Rigaku SmartLab) with CuKα (λ = 0.15405 nm) radiation at 200 mA and 45 kV. The diffraction patterns were collected in the 2θ range from 20° to 80° with a step size of 0.02° and step time of 1 s. Surface morphology and microstructure were observed using scanning-electron microscopy (SEM, Tescan VEGA3).

To confirm the presence of graphene in UHMWPE-G composites Raman spectra were acquired using a confocal Raman microscope (Horiba LabRAM HR 800 Raman Spectrometer) equipped with a diode laser at a wavelength of 488 nm and laser power of 50 mW. All Raman spectra were collected by fine-focusing with a 50× microscope objective and the data acquisition time was 10 s.

2.4 Scratch test and microhardness measurement

Scratch test was conducted as a semi-quantitative measure of the adhesion strength of thin ZrO_2 sol-gel coating on the substrate. A Rockwell C diamond indenter with a tip of 200-µm radius was used for scratching across the coating surface with the applied load increasing from 0 N to a value at which detachment of the coating occurred. Critical loads, including the load at first crack (Lc1) and the load at breakthrough (Lc2) [23-24] were determined in the scratch test. Since the sol-gel coatings in this work were transparent, reflected-light optical microscopy (OM) was used to observe the scratch tracks on the surface of different samples.

Vickers microhardness measurements for the coated and bare CoCrMo samples were

conducted using microhardness tester (Mitutoyo MicroWizhard) at a load of 0.05 kgf and a dwell time of 15 s.

2.5 Wear test

Wear testing between UHMWPE-G composites and CoCrMo samples was performed using the "linear reciprocating" test method [25] with bovine serum as the lubricating fluid. Bovine serum is the lubricant recommended by several international standards for wear testing of artificial joints and biomaterials because the wear rate and wear mechanisms closely match clinical results of polyethylene bearings [26].

The lubricant fluid in the wear test was prepared as follows. Bovine serum (supplied by Gibco) solution was first diluted to 75 % (volume fraction) using deionized water. Ethylene diamine tetra-acetic acid disodium salt (EDTA-2Na) was then added to the bovine serum solution at a concentration of 20 mM (7.45 g/L) to bind calcium in solution and to minimize precipitation of calcium phosphate on the articulating surfaces [27]. About 2% (volume fraction) of penicillin streptomycin neomycin (PSN) antibiotic mixture solution (supplied by LIFE TECHNOLOGIES EUROPE BV) was also added into bovine serum solution to suppress bacteria growth during the wear test [27].

A flat-ended circular cylinder (radius 8 mm and length 20 mm) made of UHMWPE or UHMWPE-G was used in the wear test. The flat end of the cylinder samples was polished with 1000# waterproof sandpaper before test to ensure consistent surface finish. The cylinder was pressed endwise against the CoCrMo plate with a load of 178 N applied along the longitudinal axis of the cylinder such that the average contact stress between the cylinder and the plate was about 3.5 MPa. The wear test was conducted using a wear machine (TE99 Universal Wear Machine) in the linear reciprocating mode. The samples were run through a 40-mm stroke at a rate of 2 cycle/s, producing an average sliding speed of 80 mm/s between the CoCrMo plate and the UHMWPE cylinder. Each sample was tested for 1 million cycles, and the lubricant, bovine serum solution, was changed every 0.33 million cycles. Since the wear test was carried out simultaneously with the electrochemical test (described in next section), the CoCrMo plate was sealed by epoxy so as to expose its top surface with an area of about 8 mm x 40 mm to the bovine serum.

The mass of the UHMWPE-G sample was measured before and after the wear test. Before weighing, the sample was rinsed with distilled water to remove bulk

contaminants, and cleaned in ultrasonic cleaner in distilled water for 5 min followed by drying in a dust-free environment at room temperature for 30 min.

Images of surface of samples CoCrMo, T300, T500, T700 and the counter face of the UHMWPE-G samples were captured using SEM.

2.6 Electrochemical measurements during wear tests

Electrochemical measurements of the CoCrMo samples were carried out in bovine serum at 37 °C before and during the wear test using an electrochemical workstation (PARSTAT 2263 potentiostat). Platinum plate and saturated calomel electrode (SCE) served as counter electrode and reference electrode and the CoCrMo sample was the working electrode.

All samples were immersed in bovine serum for 1 hour to electrochemically stabilize the surface before the start of wear test and electrochemical measurement. During this period the open-circuit potential (OCP) was continuously monitored. Electrochemical impedance spectroscopy (EIS) measurements were then conducted from 100000 to 0.001 Hz at a recording rate of 5 data-points per decade, with an AC amplitude of 10 mV about the OCP for the working electrode without any relative sliding motion between the plate and the cylinder. Subsequent to this, sliding wear motion was started and EIS measurements were conducted again under sliding wear.

3. Results and discussion

3.1 Characterization

3.1.1 Sol-gel ZrO_2 coating on CoCrMo

In fabricating sol-gel coating on a metallic substrate for abrasion applications, the adhesion strength of the coating is the most important measure of the coating quality. It is well known that the quality of sol-gel coating mainly depends on the sintering temperature [28-29]. In order to determine the most suitable sintering temperature, scratch test was used to semi-quantitatively measure the adhesion strength and hence to select the best sintering temperature. Fig. 1 shows typical scratch tracks of the ZrO_2 coatings under increasing load. The mean critical loads Lc1 at first crack and Lc2 at breakthrough were determined from five scratch tracks for

each coating and are given in Table 1.

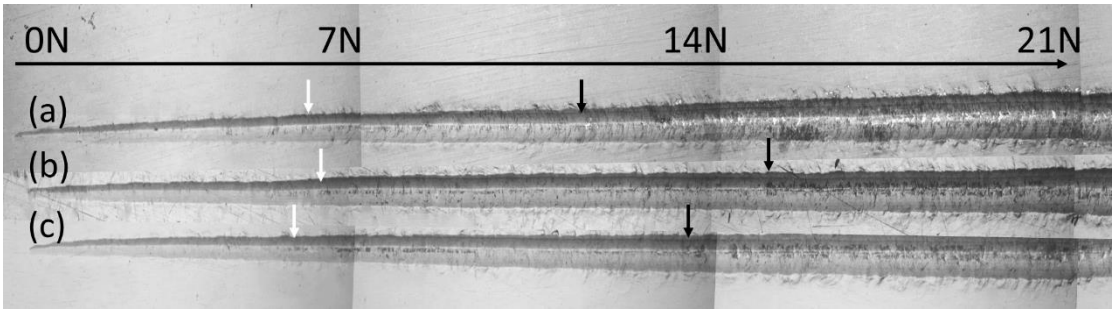

Fig. 1. Optical image of typical scratch tracks for ZrO_2 coating (a) T300, (b) T500, and (c) T700. White arrows indicate critical load at first break and dark arrows indicate critical load at breakthrough.

Sample	T300	T500	T700
Lc1(N) (first crack)	6	6	6
Lc2(N) (breakthrough)	10	15	13

Table 1. Mean critical loads in scratching test

The critical load values show that sintering at 500 °C would yield the most adherent coating. Thus sample T500 was selected for further investigation in other tests. Sol-gel stabilized zirconia coating on metals prepared at appropriate sintering temperature has been reported to result is good adhesion because its elastic modulus and thermal expansion coefficient are very close to metals such as steels and CoCr alloys [30].

Fig. 2 shows the Vickers microhardness at 0.05 kgf of the coated samples with different sintering temperatures. It can be seen that microhardness increases with sintering temperature as expected, but the adhesion strength does not. In addition, the coating, being a ceramic oxide, is much harder than the CoCrMo substrate.

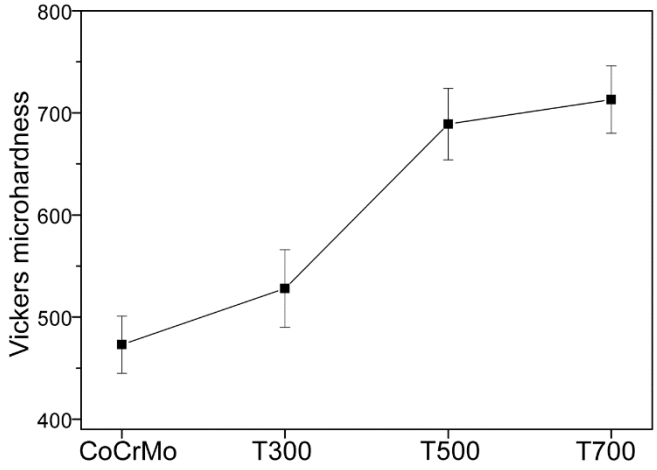

Fig.2. Vickers microhardness of CoCrMo, T300, T500 and T700 at 0.05 kgf.

The XRD patterns of CoCrMo and the coated samples are shown in Fig. 3. The XRD peaks for the CoCrMo substrate indicate that the alloy mainly consists of the HCP and FCC phase [31]. For the sol-gel coated samples T300, T500 and T700, a peak of tetragonal ZrO_2 (t-ZrO_2) begin to appear at 2θ =30.2° corresponding to the (111) lattice plane [32] when the sintering temperature is 500 °C or above. The intensity of this peak increases as the sintering temperature increases, indicating higher crystallinity as expected.

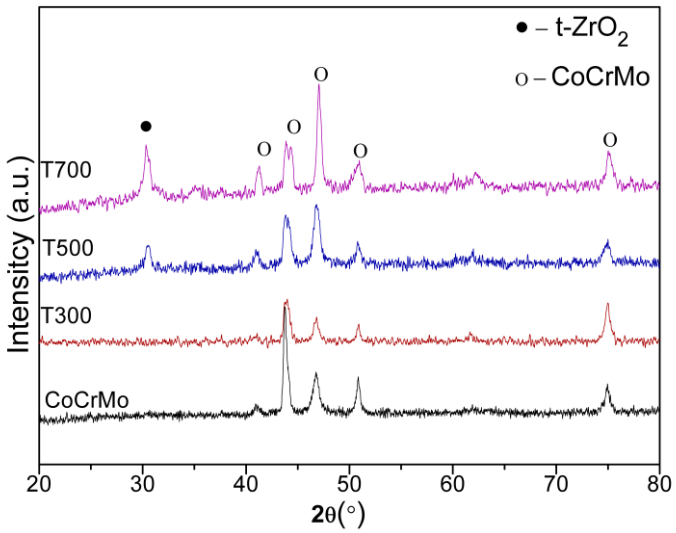

Fig. 3. XRD patterns of CoCrMo substrate and zirconia coatings sintered at different temperatures.

The surface morphology of the ZrO_2 coatings is shown in Fig. 4(a)-(c). For T300 and T500 the surface appears smooth without obvious defects. With a sintering temperature of 700 °C, some micro cracks are visible on the surface (Fig. 4(c)), indicating that this sintering temperature is too high to get an intact coating on the substrate. This is consistent with the scratching test results, which show inferior adhesion strength for T700. The cross-sectional view of T500 in Fig. 4(d) reveals a thickness of about 0.5 µm for the ZrO_2 coating on the substrate.

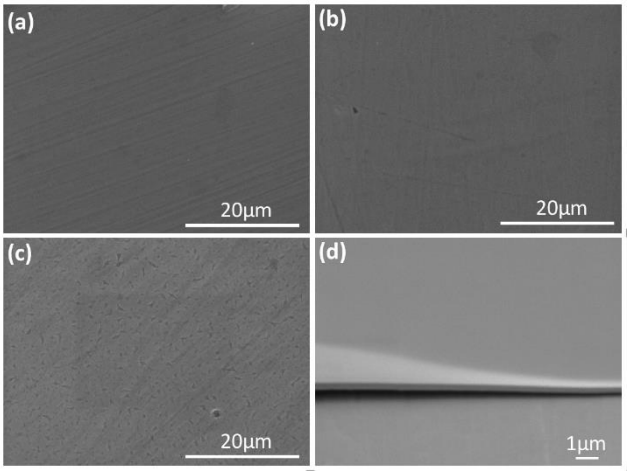

Fig. 4. SEM surface micrographs of zirconia coatings: (a) T300, (b) T500, (c) T700 and (d) cross-sectional view of T500.

3.1.2 Multi-layer graphene-reinforced polymer composite (UHMWPE-G)

In the present study the UHMWPE-G composites contain small amounts of multi-layer graphene, ranging from 0.1% to 2%. The addition of graphene in the composite, irrespective of the amount, turned the composite from white to black (Fig. 5). Such an observation on change of color is typical for polymers with addition of a carbon polymorph [33].

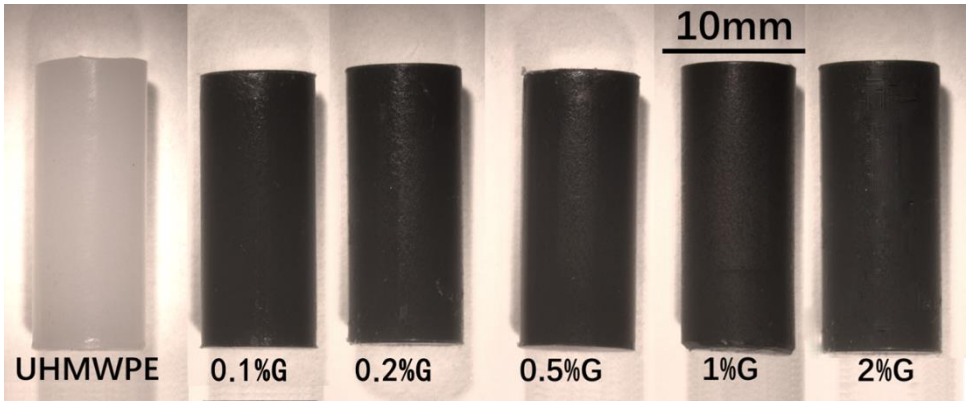

Fig. 5. Optical image of UHMWPE-G composites with different amounts (in wt%) of multi-layer graphene.

Fig. 6 shows the XRD patters of UHMWPE-G composites containing 0%, 0.1%, 0.2% and 0.5% of multi-layer graphene in the range 2θ =25°-30°. The peak at 2θ =26.7° evidences the presence of graphite-3R (003) according to PDF Card No. 26-1079.

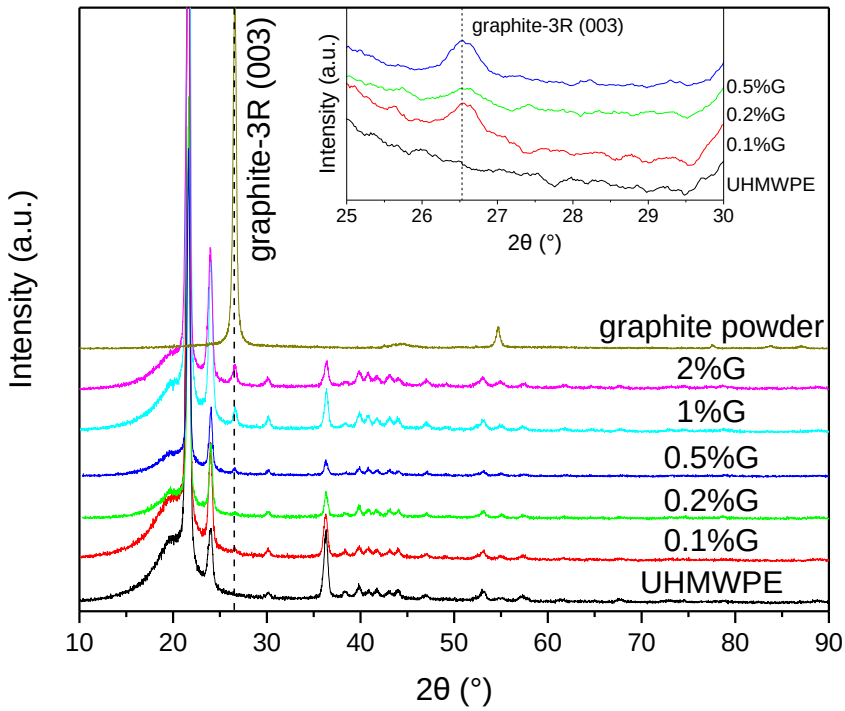

Fig. 6. XRD patterns of UHMWPE-G composites with different amounts (in wt%) of multi-layer graphene.

Fig. 7 shows the Raman spectra of the UHMWPE-G composites, with the D band (~1330 cm^{-1}) and G band (~1580 cm^{-1}) of carbon marked on the spectra. The relative peak intensity of D band to G band is often used to indicate the existence of graphene in composites [34,35]. The C-C asymmetric and symmetric stretching bands (1061 and 1128 cm^{-1}) [36], and the combination of overtones of UHMWPE between D band and G band [37], are also distinctly visible in Fig. 7.

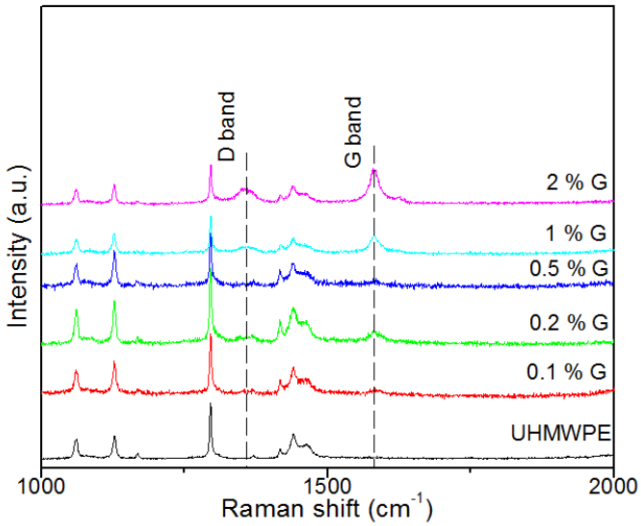

Fig.7. Raman spectra for UHMWPE-G composites with different amounts (in wt%) of multi-layer graphene.

3.2 Wear test in bovine serum

As it has been shown that sol-gel ZrO_2 coating sintered at 500 °C (designated as T500) would yield the most adherent coating based on scratching test, only T500 was subjected wear and corrosion tests in further studies against UHMWPE-G composites with different amounts of graphene reinforcement. Fig. 8 shows the mass loss in the wear test in bovine serum for 1 million cycles.

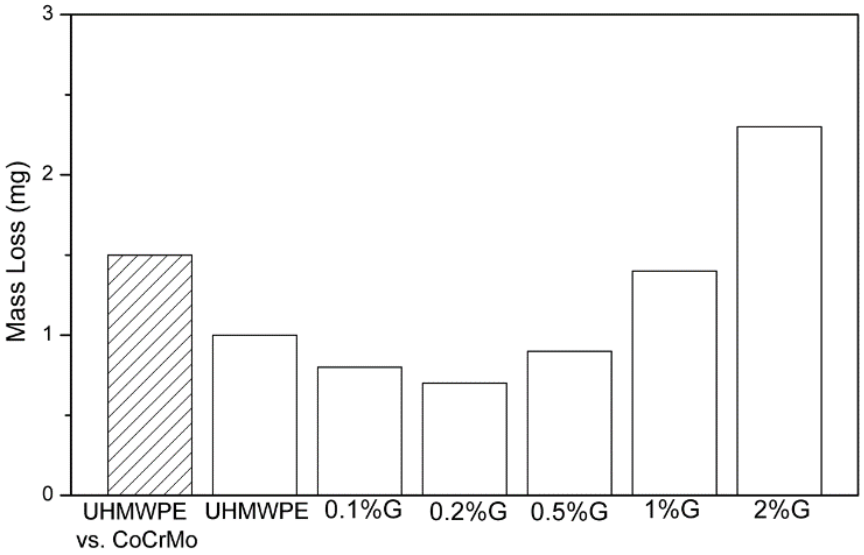

Fig.8. Wear mass loss of UHMWPE-G composites sliding against ZrO_2 coated CoCrMo sample T500 in bovine serum after one million cycles. The shaded bar, which gives the mass loss of UHMWPE against bare CoCrMo, is included for comparison.

It is clearly observed that the wear mass loss of the UHMWPE-G composite containing 0.2 % graphene is the lowest (0.7 mg). On the contrary, the mass loss of pure UHMWPE against bare CoCrMo is about 1.5 mg. This observation is consistent with the appearance of the worn surface after the wear test shown in Fig. 9. The surfaces in Fig. 9(a) and (b) are much rougher than the surfaces in Fig. 9(c) and (d).

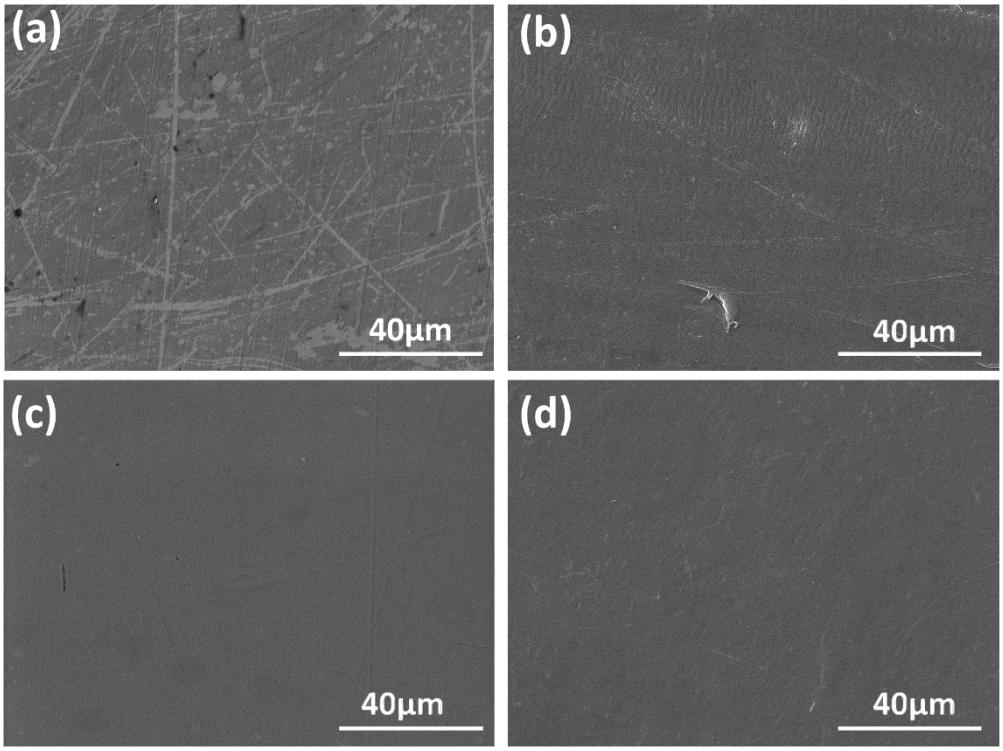

Fig.9. SEM micrographs of worn surfaces of the UHMWPE-G composites: (a) CoCrMo, (b) UHMWPE, from wear test between CoCrMo and UHMWPE; and (c) CoCrMo-ZrO_2 (T500), (d) UHMWPE-G (0.2%), from wear test between CoCrMo-ZrO_2 (T500) and UHMWPE-G (0.2%).

In the present study multi-layer graphene was added to UHMWPE to act as a reservoir of solid lubricant between the articulating surfaces since multi-layer graphene flakes possess excellent wear properties [38]. However, when more graphene was added to the polymer matrix, defects appeared on the surface of the composite. This would overshadow the lubricating effect of graphene and increase the wear mass loss (Fig. 8). The coefficient of friction for UHMWPE containing 2% of multi-layer graphene is in fact much higher, even higher than that for the untreated pair (Fig. 10), and this explains for the lower wear resistance.

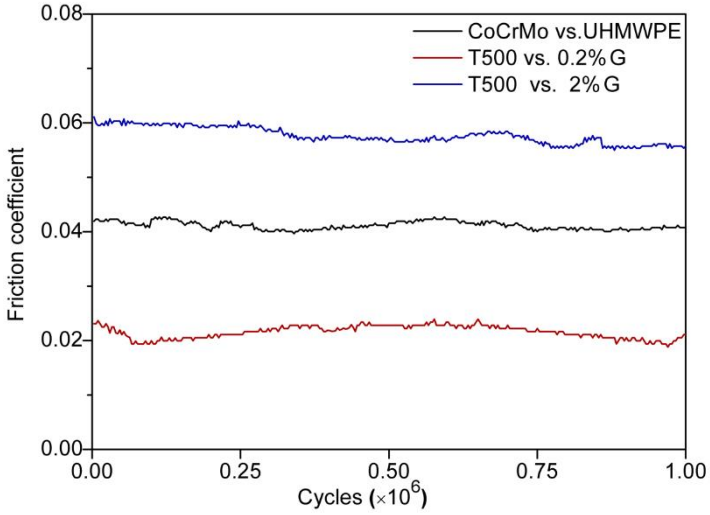

Fig. 10. Coefficient of friction for bare CoCrMo vs UHMWPE, CoCrMo-ZrO2 (T500) vs UHMWPE-G (0.2%), and CoCrMo-ZrO2 (T500) vs UHMWPE-G (2%).

Besides the lubricating effect of graphene, the anti-wear properties of zirconia compared with metallic materials also contribute to the enhanced wear performance in the modified pair CoCrMo-ZrO2 (T500) vs UHMWPE-G (0.2%) [39]. In addition, stabilized zirconia is well known for its excellent mechanical properties, including high mechanical strength and toughness [40].

3.3 Electrochemical tests in bovine serum under sliding wear

The wear loss of UHMWPE, which is the mechanically weaker component in a metal-polymer articulating pair, is a concern that shorten the service life of the pair. On the other hand, the corrosion resistance of CoCrMo under wear in an electrolyte is another concern because the protective oxide naturally grown on CoCrMo could be continuously destroyed or damaged in wearing against the counterpart. A sol-gel ceramic ZrO_2 coating, which is much thicker than naturally grown oxide film, would be more stable under wear and the substrate is protected from corrosive attack.

The open-circuit potential (OCP) for the bare and ZrO_2 coated sample before the wear test is shown in Fig. 11. Owing to the presence of the sol-gel ceramic oxide, the OCP of ZrO_2-CoCrMo (T500) is much nobler than bare CoCrMo, by about 240 mV, indicating a much more electrochemically stable surface.

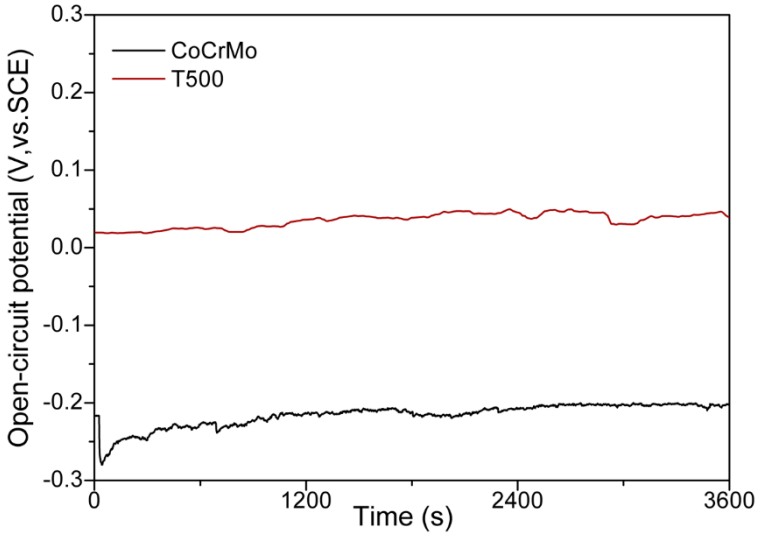

Fig. 11. Open-circuit potential of bare CoCrMo and ZrO2-CoCrMo (T500) in bovine serum at 37 °C without wearing motion.

Damage of the natural passive oxide film on bare CoCrMo would increase the corrosion rate of the metallic component and the metallic ions released could be potentially harmful [41]. To compare the corrosion resistance of bare and coated CoCrMo samples in the wear test, EIS measurement in bovine serum at 37 °C was performed before and during the wear test. Fig. 12 shows the Nyquist plot of the metallic electrodes before and during the wear test in the two wear pairs: CoCrMo against UHMWPE and ZrO2-CoCrMo (T500) against UHMWPE-G (0.2%). The plots are approximately semi-circles starting from the origin of the plot. Thus the diameter of the fitted semi-circle may be taken to be polarization resistance R_p or the corrosion resistance since R_p is inversely proportional to the corrosion current density [42].

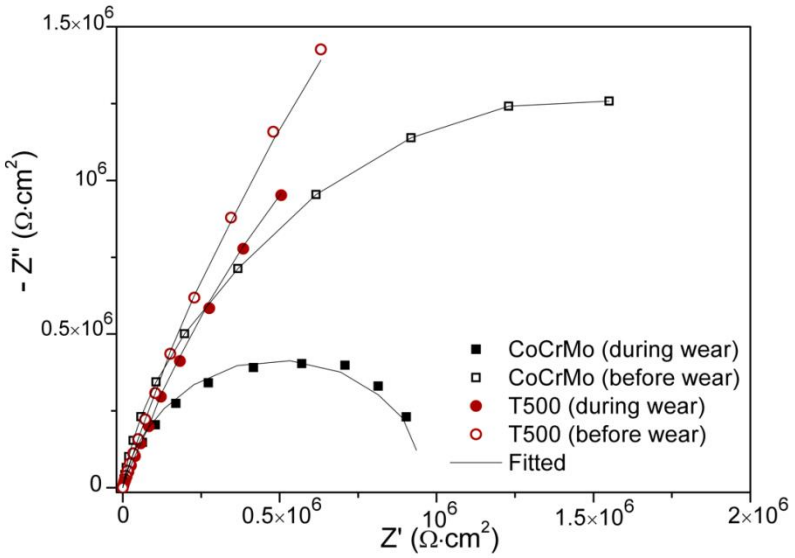

Fig. 12. Nyquist plot of metallic electrodes before and during wear test in the two wear pairs: CoCrMo against UHMWPE and ZrO_2-CoCrMo (T500) against UHMWPE-G (0.2%) in bovine serum at 37 °C.

Values of the polarization resistance R_p from the fitted curves (fitted using a commercial software ZSimpWin) in Fig. 12 are shown in Fig. 13.

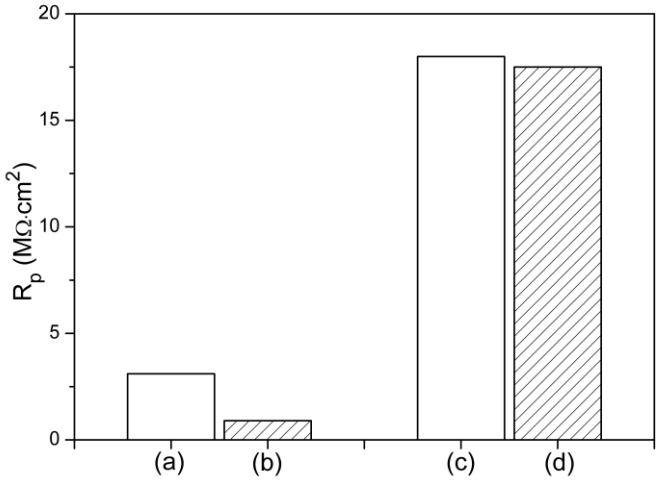

Fig. 13. Polarization resistance: Bare CoCrMo vs UHMWPE (a) before wear test (3.1 MΩ cm^2), (b) during wear test (0.90 MΩ cm^2); ZrO_2-CoCrMo (T500) vs UHMWPE-G (0.2%) (c) before wear test (18.0 MΩ cm^2)) and (d) during wear test (17.5 MΩ cm^2).

It can be seen that under quiescent condition the polarization resistance of ZrO_2-CoCrMo (T500) is about 6 times that of bare CoCrMo. More importantly, during the wear test, the polarization resistance of the coated sample only dropped slightly while that of the bare sample dropped significantly. These comparisons clearly indicate a much better corrosion resistance of the ZrO_2-coated sample, especially when abrasive motion and an electrolyte are simultaneously present.

4. Conclusions

The present study is devoted to enhancing the wear and corrosion resistance of the metal (CoCrMo) and polymer (UHMWPE) components in the presence of a simulated body fluid. In a metal-polymer pair, the polymeric component is less wear-resistant while the metallic component is less corrosion-resistant when wearing in the presence of body fluid. The performance of the metal-polymer pair was enhanced via a rational design of the two articulating components.

(1) The wear resistance of UHMWPE was improved by addition of multi-layer graphene to the polymer matrix, with graphene acting as a source of lubricant.

(2) The corrosion resistance of CoCrMo was improved by a sol-gel ZrO_2 coating sintered at a suitable temperature. This yielded an adherent coating which was thicker than the native oxide on bare CoCrMo and was also more resistant to abrasive wear.

(3) The relative performance of the CoCrMo-UHMWPE pair and the ZrO_2-CoCrMo (T500)-UHMWPE-G (0.2%) pair is summarized in Table 2 below.

	CoCrMo vs UHMWPE	ZrO_2-CoCrMo (T500) vs UHMWPE-G (0.2%)
Relative mass loss of polymer counterpart	1	0.47
Relative coeff. of friction	1	0.5
OCP of metal counterpart before wear test	-220 mV (SCE)	+20 mV (SCE)
Relative R_p of metal counterpart before wear test	1	5.81
Relative R_p of metal counterpart during wear test	0.29	5.65

Table 2. Relative performance of the CoCrMo-UHMWPE pair and the ZrO_2-CoCrMo (T500)-UHMWPE-G (0.2%) pair in bovine serum at 37 °C.

(4) The modified metal-polymer pair, that is, ZrO_2-CoCrMo (T500) vs UHMWPE-G (0.2%), is expected to be more enduring by virtue of the higher wear resistance of the polymer component and by virtue of the higher corrosion resistance of the metallic component under wear. It is clear that the present approach has not been considered from a biocompatibility standpoint. Potential applications of the present approach in biomedical implants need detailed biocompatibility evaluation in further studies.

Acknowledgements

The work described in this paper was fully supported by a grant from the Research Grants Council of the Hong Kong Special Administrative Region, China (Project No. PolyU 152219/15E). Support from the infrastructure of the Hong Kong Polytechnic University is also acknowledged.

References

[1] M. Niemczewska-Wójcik, W. Piekoszewski, The surface texture and its influence on the tribological characteristics of a friction pair: metal–polymer, Archives of Civil and Mechanical Engineering 17 (2017) 344-353. doi.org/10.1016/j.acme.2016.10.011

[2] A.V. Maksimkin, V.D. Danilov, F.S. Senatov, L.K. Olifirov, S.D.Kaloshkin, Wear performance of bulk oriented nanocomposites UHMWPE/FMWCNT and metal-polymer composite sliding bearings, Wear 392–393 (2017) 167-173. doi.org/10.1016/j.wear.2017.09.025

[3] J. Yu, Z.B. Cai, M.H. Zhu, S.X. Qu, Z.R. Zhou, Study on torsional fretting behavior of UHMWPE, App. Surf. Sci. 255 (2008) 616-618. doi.org/10.1016/j.apsusc.2008.06.179.

[4] M. Jenko, M. Gorenšek, M. Godec, M. Hodnik, B. Š. Batič, Č. Donik, J.T. Grant, D. Dolinar, Surface chemistry and microstructure of metallic biomaterials for hip and knee endoprostheses, App. Surf. Sci. 427, Part A, 1 (2018) 584-593. doi.org/10.1016/j.apsusc.2017.08.007

[5] S. Kerwell, M. Alfaro, R. Pourzal, H.J. Lundberg, Y. Liao, C. Sukotjo, L.G. Mercuri, M.T. Mathew, Examination of failed retrieved temporomandibular joint (TMJ) implants, Acta Biomaterialia 32 (2016) 324-335. doi.org/10.1016/j.actbio.2016.01.001

[6] M. Bahraminasab, B.B. Sahari, K.L. Edwards, F. Farahmand, M. Arumugam, Aseptic loosening of femoral components – Materials engineering and design considerations, Mater. Des. 44 (2013) 155–163. doi:10.1016/j.matdes.2012.07.066

[7] Y. Su, C. Luo, Z. Zhang, H. Hermawan, D. Zhu, J. Huang, Y. Liang, G. Li, L. Ren, Bioinspired surface functionalization of metallic biomaterials, J. Mech. Behav. Biomed. Mater. 77 (2018) 90–105. doi:10.1016/j.jmbbm.2017.08.035.

[8] T. Xu, L. Pruitt, Diamond-like carbon coatings for orthopaedic applications: An evaluation of tribological performance, J. Mater. Sci. Mater. Med. 10 (1999) 83–90. doi:10.1023/A:1008916903171.

[9] T.F. Zhang, B. Liu, B.J. Wu, J. Liu, H. Sun, Y.X. Leng, N. Huan, The stability of DLC film on nitrided CoCrMo alloy in phosphate buffer solution, App. Surf. Sci. 308 (2014) 100-105. doi.org/10.1016/j.apsusc.2014.04.117

[10] G. Thorwarth, C. V. Falub, U. Müller, B. Weisse, C. Voisard, M. Tobler, R. Hauert, Tribological behavior of DLC-coated articulating joint implants, Acta Biomater. 6 (2010) 2335–2341. doi:10.1016/j.actbio.2009.12.019.

[11] D. Mu, B.L. Shen, X. Zhao, Effects of boronizing on mechanical and dry-sliding wear properties of CoCrMo alloy, Mater. Des. 31 (2010) 3933–3936. doi:10.1016/j.matdes.2010.03.024.

[12] Z.J. Guo. X.L. Pang, Y. Yan, K.W. Gao, A. A. Volinsky, T.Y. Zhang, CoCrMo alloy for orthopedic implant application enhanced corrosion and tribocorrosion properties by nitrogen ion implantation, App. Surf. Sci. 347 (2015) 23-34. doi.org/10.1016/j.apsusc.2015.04.054.

[13] O. Öztürk, U. Türkan, A.E. Eroğlu, Metal ion release from nitrogen ion implanted CoCrMo orthopedic implant material, Surf. Coat. Technol. 200 (2006) 5687–5697. doi:10.1016/j.surfcoat.2005.08.113.

[14] W.W. Park, E.K. Kim, J.H. Jeon, J.Y. Choi, S.W. Moon, S.H. Lim, S.H. Han, Wear of UHMWPE against nitrogen-ion-implanted and NbN-coated Co–Cr–Mo alloy formed by plasma immersion ion implantation and deposition for artificial joints, App. Surf. Sci. 258 (2012) 8228-8233. doi.org/10.1016/j.apsusc.2012.05.026.

[15] S.P. Chenakin, V.S. FilatovaI, N. Makeeva, M.A. Vasylyev, Ultrasonic impact treatment of CoCrMo alloy: Surface composition and properties, App. Surf. Sci. 408 (2017) 11-20. doi.org/10.1016/j.apsusc.2017.03.004.

[16] Y. Liu, S.K. Sinha, Wear performances and wear mechanism study of bulk UHMWPE composites with nacre and CNT fillers and PFPE overcoat, Wear 300 (2013) 44–54. doi:10.1016/j.wear.2013.01.102.

[17] M.E. Roy, L.A. Whiteside, M.E. Magill, B.J. Katerberg, Reduced wear of cross-linked UHMWPE using magnesia-stabilized zirconia femoral heads in a hip simulator, Clin. Orthop. Relat. Res. 469 (2011) 2337–2345. doi:10.1007/s11999-011-1800-7.

[18] H. Li, Y. Xie, K. Li, L. Huang, S. Huang, B. Zhao, X. Zheng, Microstructure and wear behavior of graphene nanosheets-reinforced zirconia coating, Ceram. Int. 40 (2014) 12821–12829. doi:10.1016/j.ceramint.2014.04.136.

[19] D.S. Xiong, Y.L. Deng, N. Wang, Y.Y. Yang, Influence of surface PMPC brushes on tribological and biocompatibility properties of UHMWPE, App. Surf. Sci. 298 (2014) 56-61. doi.org/10.1016/j.apsusc.2014.01.088.

[20] F.F. He, W.Q. Bai, L.L. Li, X.L. Wang, Y.J. Xie, G. Jin, J.P. Tu, Enhancement of adhesion by a transition layer: Deposition of a-C film on ultrahigh molecular weight polyethylene (UHMWPE) by magnetron sputtering, App. Surf. Sci. 364 (2016) 280-287. doi.org/10.1016/j.apsusc.2015.12.150.

[21] W.C. Pang, Z.F. Ni, J. L. Wu, Y.W. Zhao, Investigation of tribological properties of graphene oxide reinforced ultrahigh molecular weight polyethylene under artificial seawater lubricating condition, App. Surf. Sci. 434 (2018) 273-282. doi.org/10.1016/j.apsusc.2017.10.115.

[22] C. Viazzi, J.P. Bonino, F. Ansart, Synthesis by sol-gel route and characterization of yttria stabilized zirconia coatings for thermal barrier applications, Surf. Coat. Technol. 201 (2006) 3889–3893. doi:10.1016/j.surfcoat.2006.07.241.

[23] H. Ollendorf, D. Schneider, A comparative study of adhesion test methods for hard coatings, Surf. Coat. Technol. 113 (1999) 86–102. doi:10.1016/S0257-8972(98)00827-5.

[24] W. Heinke, A. Leyland, A. Matthews, G. Berg, C. Friedrich, E. Broszeit, Evaluation of PVD nitride coatings, using impact, scratch and Rockwell-C adhesion tests, Thin Solid Films. 270 (1995) 431–438. doi:10.1016/0040-6090(95)06934-8.

[25] F732 (2011) Standard Test Method for Wear Testing of Polymeric Materials Used in Total Joint Prostheses

[26] C.J. Schwartz, S. Bahadur, Development and testing of a novel joint wear simulator and investigation of the viability of an elastomeric polyurethane for

total-joint arthroplasty devices, Wear 262 (2007) 331–339. doi:10.1016/j.wear.2006.05.018.

[27] A.P. Harsha, T.J. Joyce, Challenges associated with using bovine serum in wear testing orthopaedic biopolymers, Proc Inst Mech Eng H. 225 (2011) 948–958. doi:10.1177/0954411911416047.

[28] K. Joy, I.J. Berlin, P.B. Nair, J.S. Lakshmi, G.P. Daniel, P.V. Thomas, Effects of annealing temperature on the structural and photoluminescence properties of nanocrystalline ZrO2 thin films prepared by sol–gel route, J. Phys. Chem. Solids. 72 (2011) 673–677. doi:10.1016/j.jpcs.2011.02.012.

[29] M.K. Ahmad, N.A. Rasheid, A.Z. Ahmed, S. Abdullah, M. Rusop, Effect of Annealing Temperature on Titanium Dioxide Thin Films Prepared by Sol Gel Method, AIP Conf. Proc. 1017 (2008) 109. doi:10.1063/1.2940607.

[30] R. Di Maggio, A. Tomasi, P. Scardi, Characterisation of thin ceramic coatings on metal substrates, Mater. Lett. 31 (1997) 345–349. doi:10.1016/S0167-577X(96)00298-4.

[31] X. Zhang, Y. Li, N. Tang, E. Onodera, A. Chiba, Corrosion behaviour of CoCrMo alloys in 2 wt% sulphuric acid solution, Electrochim. Acta. 125 (2014) 543–555. doi:10.1016/j.electacta.2014.01.143.

[32] S.K. Tiwari, J. Adhikary, T.B. Singh, R. Singh, Preparation and characterization of sol-gel derived yttria doped zirconia coatings on AISI 316L, Thin Solid Films 517 (2009) 4502–4508. doi:10.1016/j.tsf.2008.12.025.

[33] K. V Dorozhkin, G.E. Dunaevsky, S.Y. Sarkisov, V.I. Suslyaev, O.P. Tolbanov, V.A. Zhuravlev, Y.S. Sarkisov, V.L. Kuznetsov, S.I. Moseenkov, N. V Semikolenova, V.A. Zakharov, V. V Atuchin, Terahertz dielectric properties of multiwalled carbon nanotube/polyethylene composites, Mater. Res. Express. 4 (2017) 106201. doi:10.1088/2053-1591/aa8f06.

[34] L.M. Malard, M.A. Pimenta, G. Dresselhaus, M.S. Dresselhaus, Raman spectroscopy in graphene, Phys. Rep. 473 (2009) 51–87. doi:10.1016/j.physrep.2009.02.003.

[35] A.C. Ferrari, Raman spectroscopy of graphene and graphite: Disorder, electron-phonon coupling, doping and nonadiabatic effects, Solid State Commun. 143 (2007) 47–57. doi:10.1016/j.ssc.2007.03.052.

[36] R.P. Wool, R.S. Bretzlaff, B.Y. Li, C.H. Wang, R.H. Boyd, Infrared and raman spectroscopy of stressed polyethylene, J. Polym. Sci. Part B Polym. Phys. 24 (1986) 1039–1066. doi:10.1002/polb.1986.090240508.

[37] M.J. Gall, P.J. Hendra, O.J. Peacock, M.E.A. Cudby, H.A. Willis, The laser-Raman spectrum of polyethylene: The assignment of the spectrum to fundamental modes of vibration, Spectrochim. Acta Part A Mol. Spectrosc. 28 (1972) 1485–1496. doi:10.1016/0584-8539(72)80118-1.

[38] M. Poot, H.S.J. van der Zant, Nanomechanical properties of few-layer graphene membranes, Appl. Phys. Lett. 92 (2008) 063111. doi:10.1063/1.2857472.

[39] I. Piwoński, K. Soliwoda, A. Kisielewska, R. Stanecka-Badura, K. Kądzioła, The effect of the surface nanostructure and composition on the antiwear properties of zirconia-titania coatings, Ceram. Int. 39 (2013) 1111–1123. doi:10.1016/j.ceramint.2012.07.034.

[40] P.F. Manicone, P.R. Iommetti, L. Raffaelli, An overview of zirconia ceramics: Basic properties and clinical applications, J. Dent. 35 (2007) 819–826. doi:10.1016/j.jdent.2007.07.008.

[41] A. Sargeant, T. Goswami, Hip implants: Paper V. Physiological effects, Mater. Des. 27 (2006) 287–307. doi:10.1016/j.matdes.2004.10.028.

[42] D. A. Jones, *Principles and Prevention of Corrosion*, 2nd Edition, Ch. 3, Ch. 5, 1996, Prentice-Hall, US

List of Table and Figure captions

Table 1. Mean critical loads in scratching test.

Table 2. Relative performance of the CoCrMo-UHMWPE pair and the ZrO_2-CoCrMo (T500)-UHMWPE-G (0.2%) pairs in bovine serum at 37 °C.

Fig. 1. Optical image of typical scratch tracks for ZrO2 coating (a) T300, (b) T500, and (c) T700. White arrows indicate critical load at first break and dark arrows indicate critical load at breakthrough.

Fig.2. Vickers microhardness of CoCrMo, T300, T500 and T700 at 0.05 kgf.

Fig. 3. XRD patterns of CoCrMo substrate and zirconia coatings sintered at different temperatures.

Fig. 4. SEM surface micrographs of zirconia coatings: (a) T300, (b) T500, (c) T700 and (d) cross-sectional view of T500.

Fig. 5. Optical image of UHMWPE-G composites with different amounts (in wt%) of multi-layer graphene.

Fig. 6. XRD patterns of UHMWPE-G composites with different amounts (in wt%) of multi-layer graphene.

Fig.7. Raman spectra for UHMWPE-G composites with different amounts (in wt%) of multi-layer graphene.

Fig.8. Wear mass loss of UHMWPE-G composites sliding against ZrO_2 coated CoCrMo sample T500 in bovine serum after one million cycles. The shaded bar, which gives the mass loss of UHMWPE against bare CoCrMo, is included for comparison.

Fig.9. SEM micrographs of worn surfaces of the UHMWPE-G composites: (a) CoCrMo, (b) UHMWPE, from wear test between CoCrMo and UHMWPE; and (c) CoCrMo-ZrO_2 (T500), (d) UHMWPE-G (0.2%), from wear test between CoCrMo-ZrO_2 (T500) and UHMWPE-G (0.2%).

Fig. 10. Coefficient of friction for bare CoCrMo vs UHMWPE, CoCrMo-ZrO2 (T500) vs UHMWPE-G (0.2%), and CoCrMo-ZrO2 (T500) vs UHMWPE-G (2%).

Fig. 11. Open-circuit potential of bare CoCrMo and ZrO2-CoCrMo (T500) in bovine serum at 37 °C without wearing motion.

Fig. 12. Nyquist plot of metallic electrodes before and during wear test in the two wear pairs: CoCrMo against UHMWPE and ZrO2-CoCrMo (T500) against UHMWPE-G (0.2%) in bovine serum at 37 °C.

Fig. 13. Polarization resistance of bare and coated CoCrMo before and during wear test.